

# Multifrequency Printed Antennas Loaded with Metamaterial Particles

Daniel SEGOVIA-VARGAS<sup>1</sup>, Francisco Javier HERRAIZ-MARTÍNEZ<sup>1</sup>,  
Eduardo UGARTE-MUÑOZ<sup>1</sup>, Javier MONTERO-DE-PAZ<sup>1</sup>,  
Vicente GONZÁLEZ-POSADAS<sup>2</sup>, Luis Enrique GARCÍA-MUÑOZ<sup>1</sup>

<sup>1</sup> Dept. of Signal Theory and Communications, Carlos III University in Madrid,  
Avenida de la Universidad 30, 28911 Leganés, Madrid, Spain

<sup>2</sup> Departamento de Ingeniería Audiovisual y Comunicaciones, Universidad Politécnica de Madrid, Madrid, Spain

dani@tsc.uc3m.es, fjherraiz@tsc.uc3m.es

**Abstract.** *This paper provides a review of printed antennas loaded with metamaterial particles. This novel technique allows developing printed antennas with interesting features such as multifrequency (simultaneous operation over two or more frequency bands) and multifunctionality (e. g. radiation pattern diversity). Moreover, compactness is also achieved and the main advantages of conventional printed antennas (light weight, low profile, low cost ...) are maintained. Different types of metamaterial-loaded printed antennas are reviewed: printed dipoles and patch antennas. Several prototypes are designed, manufactured and measured showing good results. Furthermore, simple but accurate equivalent models are proposed. These models allow an easy and quick design of metamaterial-loaded printed antennas. Finally, two interesting applications based on the proposed antennas are reviewed: the patch antennas are used as radiating elements of emerging active RFID systems in the microwave band and the metamaterial-loaded printed dipoles are employed to increase the performance of log-periodic arrays.*

## Keywords

Printed antennas, metamaterials, multifrequency antennas, multifunction antennas.

## 1. Introduction

Wireless communication systems have grown dramatically in the last few years. These systems have a great penetration on the society. Several examples can be mentioned: mobile communications (GSM, DCS, UMTS), personal area networks (Bluetooth), local area wireless networks (WiFi), radio navigation systems (GPS, Galileo), etc. Related to this fact, the popularity and sales of wireless terminals have also grown. The first user terminals which become so popular were mobile phones. However, mobile phones are not the only user terminals extended in the

society. We have several examples: PDAs, laptops and more recently terminals embedded inside cars.

Initially, the user terminals were devoted to only one service and standard (e. g. GSM mobile phones) [1]. After that, the necessity of providing several standards with only one terminal arose (e. g. multi-band mobile phones, such as [1] or [3]). This implies the use of antennas working at several frequencies simultaneously. Moreover, the use of a single terminal for several communication systems is becoming more and more common. For example, mobile phones and PDAs are currently user terminals for mobile communication systems and GPS and they also provide Bluetooth connectivity; terminals embedded in cars provide radio navigation services (GPS) and Bluetooth connectivity, etc. It is important to note that the requirements of the terminals for such different services are different. For example, the radiation patterns of an antenna for mobile systems and radio navigation systems are orthogonal. Thus, multifunctionality is the main requirement for antennas in modern handsets [4]. Moreover, these antennas must be compact in order to fit them into handheld devices.

Most of the wireless systems are based on two functional elements: the user terminal and the base station [1]. Previously we have considered the importance of the radiating element from the terminal point of view, but it is important to note that proper selection of the antenna installed in the provider element (base-station, hot-spot, etc.) is crucial in order to achieve an optimal performance of the wireless system. From the technical point of view, it is necessary to develop multifrequency antennas with several working bands but also other characteristics must be provided. For example, the new versions of WiFi and future mobile systems propose the use of diversity [5], [6]. Moreover, the proliferation of base-stations for communication systems was criticized by several social groups. Multifrequency antennas for base-station can reduce the number of these system elements, reducing the social alarm. Furthermore, the same considerations about the cost and size which were made for the user terminals can be applied here.

Current solutions, such as broadband antennas and conventional resonant antennas, are not optimal. On one hand, broadband antennas have a broad bandwidth which can cover all the working frequencies [7], [8], but they also work at undesired bands receiving undesired interferences. On the other hand, conventional resonant antennas can be used at several frequencies but the ratio between them is harmonic [9], [10] (an integer number equal to or larger than two) while the ratio between current services is anharmonic and smaller than 2 in most of the cases. For this reason, a broad range of novel antennas has to be developed to fulfill the requirements of modern communication systems and emerging applications, such as Radio-Frequency Identification (RFID) systems [11]. All these requirements cannot be achieved with conventional approaches. This fact has made that novel technologies are being studied and implemented. One of these technologies is the use of metamaterial structures.

Metamaterials are one of the hot topics in the fields of physics and engineering [12] - [15]. This is clear since the number of scientific publications, conferences and seminars devoted to this topic has grown exponentially during the last years. This fact has made that there is no unique definition of metamaterials. Anyway, metamaterials can be broadly defined as electromagnetic structures engineered to achieve exotic or unusual properties.

These features have been used in microwave engineering to develop devices with extraordinary properties such as miniaturization or operation over multiple frequency bands [12], [13]. On the other hand, the effort in the antenna field has been put on the use of metamaterials for travelling-wave antennas [13], [14], and as substrates and superstrates for antennas [13]-[15]. Recently, there has been a great effort on miniaturized antennas based on metamaterial concepts [13]-[15].

Nevertheless, from the authors' point of view, the possibility of achieving multifrequency and/or multifunction antennas based on metamaterials has not been fully explored. Moreover, these features can be combined with the possibility of miniaturization to develop compact antennas for modern and future wireless communication systems.

During the last thirty years printed technology has been the most popular technique to manufacture antennas [9], [10]. Printed antennas have become so popular due to their low profile, light weight, low cost, simplicity to integrate with circuitry and usefulness as elements of antenna arrays.

Recently, the authors have proposed printed antennas loaded with metamaterial particles in order to achieve multifrequency and multifunction antennas [16], [17]. It has been shown that these features can be achieved by loading a printed antenna with a small number of metamaterial particles. Thus, the size, cost and complexity of the original antennas are not increased.

The main aim of this paper is to explain the behavior of these printed antennas loaded with metamaterial particles and demonstrate their performance by means of measured prototypes. Moreover, simple models of these antennas based on equivalent circuit and transmission line (TL) approaches are presented. These models allow designing the proposed antennas easily and quickly without losing accuracy. Then, this paper will firstly deal with wire antennas loaded with metamaterial particles, secondly with patches loaded with Sievenpiper mushroom or split ring resonator and finally with some applications related to some hot topics, i.e. RFID.

The detailed organization of the present paper is as follows: multifrequency printed dipoles loaded with metamaterial particles are presented in Section 2. The design guidelines and an equivalent circuit model are proposed. Several prototypes are manufactured and measured, showing good results. The third Section is devoted to multifrequency patch antennas. Two kinds of patches are proposed: the first one is based on patches partially filled with metamaterial structures, while the other one consists of metamaterial particles coupled to patch antennas. These patch antennas can be used for different applications: the first one is more suitable for wireless handhelds (communications band: 1 GHz-3 GHz) while the second one is proposed for satellite applications (X band). Simple but accurate models are proposed for both kinds of patches and several prototypes are presented. In Section 4, some specific applications of the proposed multifrequency printed antennas are reviewed: the proposed antennas can be used as the radiating elements of emerging systems like RFID and they can be used to increase the features of antenna arrays. Finally, this paper is concluded in Section 5.

## 2. Printed Dipoles Loaded with Metamaterial Particles

### 2.1 Proposed Approach and Dual-Frequency Examples

The geometry of the proposed multifrequency dipoles is based on an antipodal printed dipole loaded with metamaterial particles. This antipodal dipole is printed on both sides of a dielectric substrate with the height  $h$ . The parameters of the dipole are the length of each branch  $L$  and the width  $W$ . This configuration has been chosen because it avoids the use of a balun to feed the antenna. This is possible because the printed dipole is fed through a paired strips transmission line [18] with a SMA connector soldered to the end of the line. The outer conductor of the SMA connector is soldered to one strip while the inner conductor is soldered to the other strip of the feeding line. The dimensions of the feeding line are the length  $L_f$  and the width  $W_f$ .

One metamaterial particle or a set of them are coupled to each branch of the dipole. In the case of Fig. 1, four SRRs are printed on the opposite side of each dipole branch. This configuration has been chosen because it provides a proper matching within a wide range of ratios between the working frequencies. The SRRs parameters, according to Fig. 1 (b), are the external radius  $R$ , the width of the strips  $W_{SRR}$  and the gap between strips  $g$ . The SRRs are placed at a distance  $c$  from the dipole centre. The separation between the centers of the SRRs is  $s$ . In addition, other metamaterial particles can be used to obtain the desired multifrequency performance (spiral resonators, Omega particles ...). Regardless of the particular configuration, the metamaterial particles must be located in a way such the magnetic field generated by the currents through the dipole branches has an important component in the direction perpendicular to the plane of the particles. This is similar to the case of TLs loaded with metamaterial particles [12].

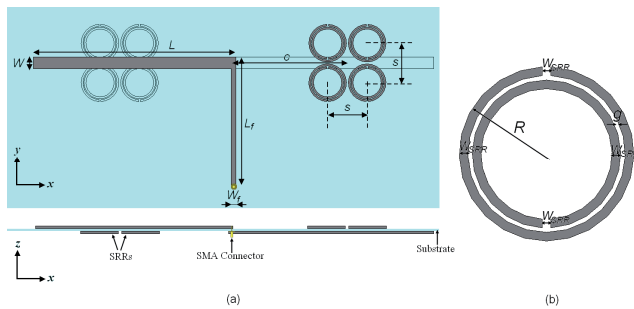


**Fig. 1.** Sketch of the proposed antenna: (a) Top and side views of the SRRs-loaded dipole antenna with its design parameters. (b) Split Ring Resonator parameters.

A prototype of the proposed SRRs-loaded dipole antenna has been designed. The dimensions of the dipole are:  $L=42.05$  mm,  $W=2.50$  mm,  $L_f=27.5$  mm and  $W_f=1.00$  mm. The low-cost FR-4 substrate ( $h=0.50$  mm,  $\epsilon_r=4.50$  and  $\tan \delta=0.015$ ) has been used. The prototype is loaded with a set of four SRRs per branch, placed at a distance  $c=24.20$  mm and the separation  $s$  is 8.40 mm. The parameters of the SRRs are the radius  $R=4.00$  mm, the width  $W_{SRR}=0.40$  mm and the gap between rings  $g=0.20$  mm. The theoretical resonant frequency of the unloaded antipodal dipole with these dimensions is 1.53 GHz, considering the fundamental mode. According to [19] the resonant frequency of the SRRs is 2.55 GHz.

The proposed configuration provides the desired dual-frequency performance. The first frequency ( $f_1$ ) is close to the fundamental frequency of the dipole ( $n=+1$  mode) while the additional frequency ( $f_{SRR}$ ) occurs in the vicinity of the SRRs self-resonant frequency. Fig. 2 (b)-(c) (obtained with Momentum) shows the current distributions on the proposed dipole at the two working frequencies. At  $f_1$  (Fig. 2 (a)) the current distribution is similar to the one obtained in the conventional  $\lambda/2$  dipole (Fig. 2 (a)). It can be appreciated that the effect of the SRRs at this frequency is negligible and nearly no current passes along them. This

implies that the expected radiation pattern at this frequency is also similar to the reference dipole. In fact, the only modification in the antenna performance is a very slight frequency shift in the resonant frequency towards lower frequencies due to the capacitive parasitic effect of the SRRs. On the other hand, the working principle at  $f_{SRR}$  is somewhat different since the resonant frequency is imposed by the SRRs. At this frequency the SRRs are resonating as can be seen in Fig. 2 (c) where the currents through the SRRs are maximum. In this case the SRRs are not radiating but imposing a hard boundary condition (an open circuit) where they are placed. In this way the currents in the dipole are nearly zero from this position to the end of the overall dipole. This means that the radiating element is formed by the current distribution on the dipole between the SRRs arrangements. It should be noted that this radiating element is a dipole with a length shorter than  $\lambda/2$  sustaining a uniform current between the edges where the SRRs are placed. Thus, it is expected that the proposed structure gives a dipolar-like radiation pattern at  $f_{SRR}$ . This is an important feature because the proposed dipoles not only present the desired dual-frequency performance but they keep the dipolar-like radiation pattern at both working frequencies.

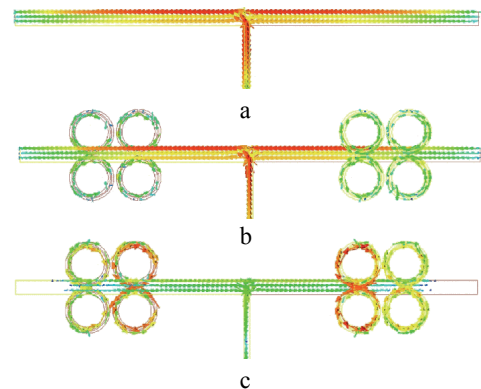


**Fig. 2.** (a) Currents on the unloaded dipole at the fundamental frequency. (b) Currents on the SRRs-loaded dipole at  $f_1$ . (c) Currents on the SRRs-loaded dipole at  $f_{SRR}$ .

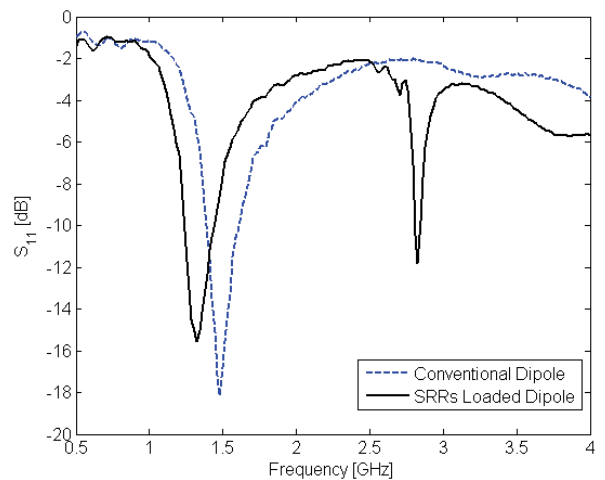


**Fig. 3.** Measured reflection coefficients of the conventional and the dual-band SRR-loaded printed dipoles.

The proposed dual-frequency dipole and the conventional unloaded dipoles have been manufactured. The measured reflection coefficients of both prototypes are shown in Fig. 3. The reference dipole working frequency is 1.48 GHz, while the proposed SRRs-loaded dipole presents the desired dual-frequency performance. The first resonance appears at  $f_1 = 1.32$  GHz. At this frequency the current along the SRRs is negligible and the only effect of the SRRs is to slightly shift down the frequency of the proposed dipole. The second working frequency ( $f_{SRR}$ ) is 2.83 GHz, which is very close to the SRRs self-resonance frequencies. This frequency is shifted towards higher frequencies due to the overall effect of the SRRs coupled to the dipole and the tolerances of the substrate and the manufacturing process. The bandwidth at the lower band is around 15% at the -10 dB level for both dipoles. On the other hand, the bandwidth at the additional band (at the -10 dB level) for the proposed dipole is much lower (1.27%). This is due to the high Q factor of the SRRs, what implies a much smaller bandwidth in the resonance imposed by them.

Fig. 4 shows the measured radiation patterns of the proposed dual-frequency dipole at both working frequencies (1.32 GHz and 2.83GHz). Both of them are dipolar and similar to the conventional dipole. A ripple can be noticed especially at the YZ plane because of the presence of a metallic plate, part of the positioner, behind the antenna. The measured gain of the reference dipole is 1.99 dB while the gain of the dual-frequency prototype is 1.81 dB at  $f_1$  and 0.67 dB at  $f_{SRR}$ .

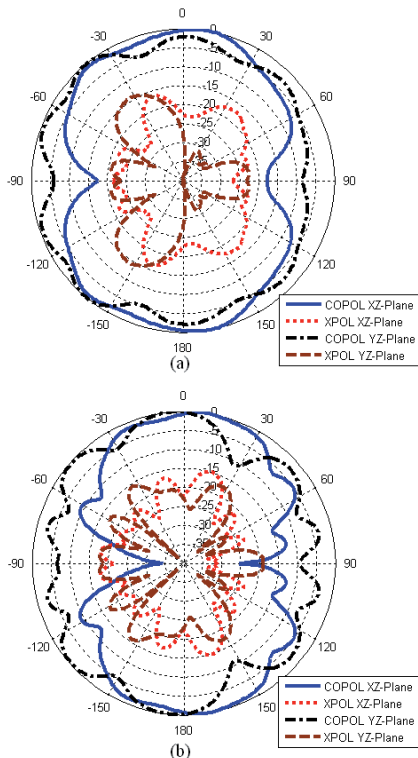


Fig. 4. Measured radiation patterns of the proposed SRR-loaded dipole. (a)  $f_1 = 1.32$  GHz, (b)  $f_{SRR} = 2.83$  GHz.

In the previous case, the additional frequency is placed above the resonant frequency of the unloaded dipole, but it is possible to excite the additional frequency below the resonant frequency of the unloaded dipole with the proposed approach. An example of the later is shown below.

The dipole implementation is based on the antipodal dipole printed on both sides of a dielectric substrate with the height  $h$ . A dipole with  $L = 28.50$  mm,  $W = 3.00$  mm,  $L_f = 36.50$  mm and  $W_f = 1.00$  mm is considered. The substrate is the low-cost FR-4 ( $\epsilon_r = 4.50$  and  $\tan \delta = 0.015$ ) with  $h = 0.50$  mm. The resonant frequency of the fundamental mode of this dipole is 2.12 GHz.

The previous dipole is loaded with an Omega particle per branch (Fig. 5). The dimensions of each omega particle are:  $L_p = 4.60$  mm,  $W_p = 3 \cdot L_p = 13.80$  mm and  $W_s = 0.40$  mm. These particles are coupled at the centre of the branches. The separation gap between the particles and the dipole is 0.20 mm.

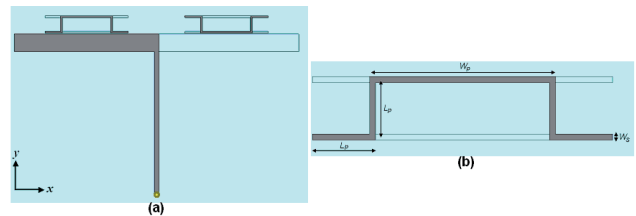


Fig. 5. Sketches of the Omega-loaded antipodal printed dipole. (a) Top view. (b) Design parameters of the Omega particles.

Fig. 6 shows the reflection coefficient of the loaded and unloaded dipoles. The unloaded dipole has its fundamental resonance at 2.12 GHz, as expected. On the other hand, the loaded dipole has two resonances: the first one at 1.70 GHz, while the second one at 2.21 GHz. This second resonance is the resonance of the dipole which has been slightly shifted up towards higher frequencies due to the parasitic effect of the particles. The first one is the additional resonance produced by the Omega particles. It is important to note that this resonance is obtained below the resonant frequency of the fundamental mode of the dipole. This is opposite to the example presented before. This demonstrates that the additional resonances can be completely controlled by choosing the adequate particles. The electrical length of the dipole at the first resonant frequency is  $0.32\lambda_0$ , while it is  $0.42\lambda_0$  at the second frequency. This means that miniaturization is achieved for the first frequency. The ratio between the working frequencies is only 1.3, which cannot be achieved with other approaches.

The radiation patterns at the two working frequencies are shown in Fig. 7. In both cases, the dipolar radiation pattern is obtained. The computed gain is 1.06 dB at the first frequency, while it is 1.99 dB at the second one. The gain is smaller at the first frequency because the electrical length of the antenna is also smaller.

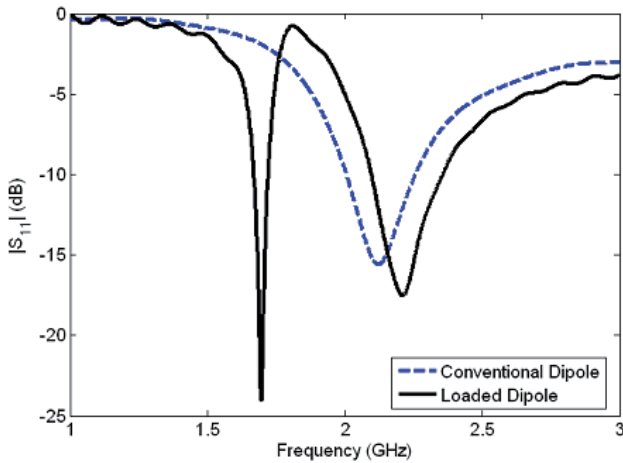


Fig. 6. Measured reflection coefficient of the Omega-loaded and unloaded dipoles.

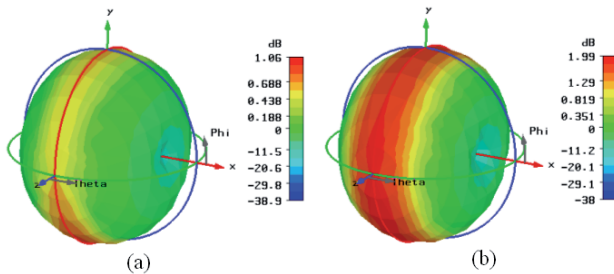


Fig. 7. Simulated radiation patterns of the proposed dual-band antipodal dipole loaded with Omega particles. (a) 1.70 GHz. (b) 2.21 GHz.

### 2.2 Multifrequency Printed Dipoles

The approach to obtain multifrequency printed dipoles (printed dipoles with three or more working frequencies) consists of exciting two or more additional resonances. These additional resonances are obtained with different pairs of metamaterial particles. At least one of each pair of metamaterial particles must resonate at a desired additional frequency. As an example, a triple-frequency printed dipole is proposed below.

According to Fig. 8, let us consider the case in which  $R_2 = R_1 + 0.4$  mm. In this case, the resonant frequencies of the SRRs above and below the dipole are separated 0.22 GHz and a triple-frequency antenna can be obtained.



Fig. 8. Sketch of the proposed triple-frequency printed dipole.

Fig. 9 shows the simulated (CST®) reflection coefficient for the proposed triple-frequency antenna. The three working frequencies can be easily identified. The  $|s_{11}|$  parameters of the dipoles loaded with both SRRs with  $R = R_1$  and  $R = R_2$  are also plotted. These plots show that the three

resonances of the triple-frequency antenna are due to the self-resonant frequencies of the dipole and the SRRs with different dimensions.

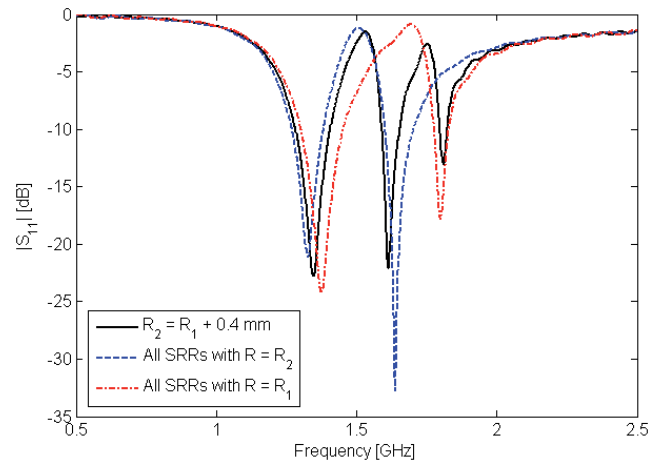


Fig. 9.  $|s_{11}|$  parameter of the triple-frequency printed dipole antenna. The same information for the cases in which all the SRRs have the same dimensions is also plotted.

The simulated currents on the antenna at the three working frequencies are shown in Fig. 10. The distributions are similar to the one presented by the dual-frequency dipole (Fig. 2). The SRRs are not resonating at the first working frequency ( $f_1$ ) and the currents on the dipole are similar to the unloaded dipole. The SRRs with  $R_2$  are resonating at the second working frequency ( $f_2$ ). Most of the current on the dipole is between the SRRs and there is almost no current between the SRRs and the edges of the dipole. At the third working frequency ( $f_3$ ) the distribution is similar to the previous one ( $f_2$ ) but the SRRs with  $R_1$  are resonating instead of  $R_2$ -SRRs. The radiation pattern is dipolar at the three working frequencies.

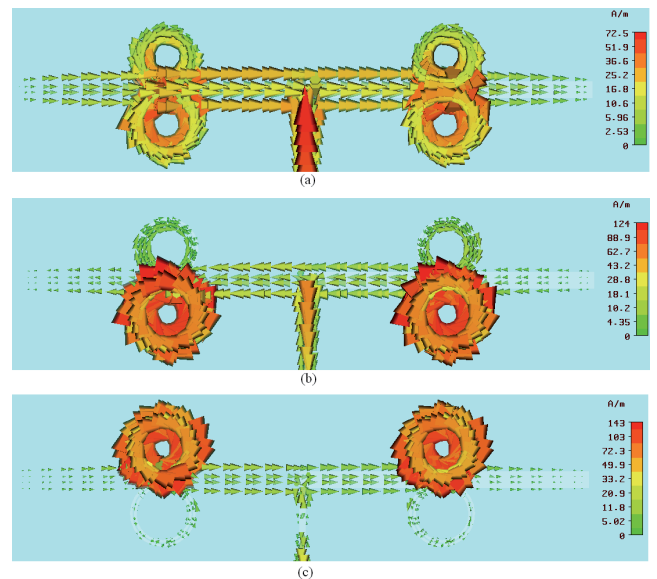


Fig. 10. Currents on the triple-frequency printed dipole loaded with SRRs. (a)  $f_1$  (fundamental frequency of the unloaded dipole). (b)  $f_2$  (resonant frequency of the SRRs with  $R_2$ ). (c)  $f_3$  (resonant frequency of the SRRs with  $R_1$ ).

### 2.3 Equivalent Circuit Model

Fig. 11 shows the proposed equivalent circuit model for metamaterial-loaded printed dipoles. As it was demonstrated in [19], basic metamaterial particles, such as SRRs or spirals, can be modeled as LC parallel resonators. For this reason, a resonator is placed in series with each dipole branch in the corresponding antenna model. The coupled resonator is modeled by the following parameters: the unloaded quality factor  $Q$ , the coupling factor  $\beta$  (ratio between the unloaded quality factor and the external quality factor), the resonant frequency  $f_0$ , and a small capacitance  $C_a$ . This last capacitance is due to the common area between the SRRs and the dipole branches. The effect of this capacitance is to model the slight shift of the resonant frequency of the dipole due to the coupling effects. This circuit model can be used for any configuration of the metamaterial-loaded dipoles (one, two or four SRRs per branch, spiral resonators, Omega particles, etc.) by only choosing adequately the parameters of the equivalent circuit. Moreover, it can be also used when two or more additional resonances are obtained. In that case, for each additional resonance another coupled resonator per branch must be added to the model.

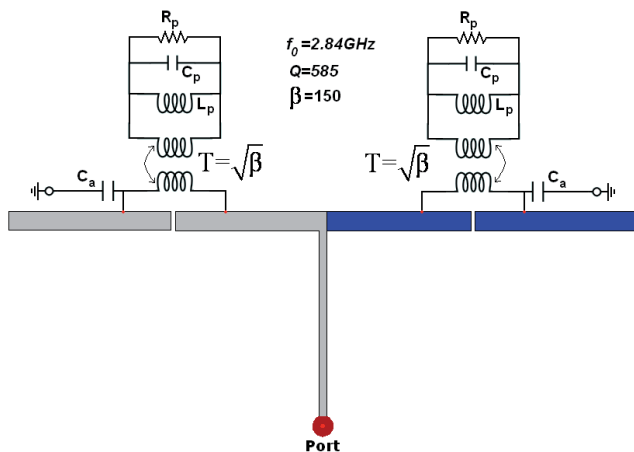


Fig. 11. Equivalent circuit model of the metamaterial-loaded printed dipoles.

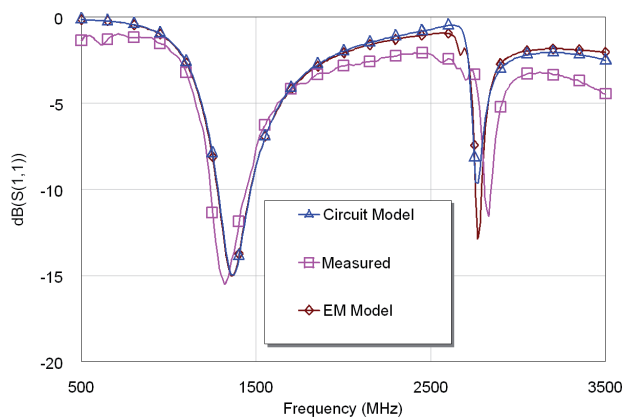


Fig. 12. Reflection coefficient of the dual-band SRR-loaded dipole computed with the equivalent circuit model and the FW simulator. The measured reflection coefficient is also plotted.

In order to show the validity of the proposed model, the prototype presented in the previous Subsection has been simulated with the proposed model and a full-wave electromagnetic simulator (Momentum). The adequate parameters for the proposed prototype are: the unloaded  $Q = 327$ ,  $f_0 = 2.71$  GHz,  $\beta = 95$ ,  $C_a = 0.11$  pF. An excellent agreement between the measurements, the full-wave simulator and the proposed model results can be seen in Fig. 12.

### 3. Multifrequency and Multifunction Microstrip Patch Antennas

Microstrip patch antennas are very popular radiators due to their low profile, light weight, low cost, easiness of manufacturing and integrating with circuitry [9], [10]. However, conventional single patches cannot be used as multifrequency antennas due to the fact that the multifrequency performance comes from higher order modes with multi-lobe radiation patterns. The most common ways of obtaining multifrequency performance with patch antennas are: the stacking of two or more patches with different resonant frequencies (leading to multilayer structures) and the addition of parasitic elements [9], [10]. Both of these techniques imply an increase of size instead of a reduction. Metamaterial structures can be used to develop simultaneous multifrequency patch antennas in which size reduction is also achieved.

One of the main applications of metamaterial structures is the development of Left-Handed (LH) Transmission Lines (TLs) [13]. These TLs allow the propagation of backward-waves, which means that the phase and group velocities are antiparallel ( $v_g \cdot v_p < 0$ ). If we consider a TL as the concatenation of infinite unit cells, the equivalent circuit model of a LH unit cell is the dual of a conventional or Right-Handed (RH) unit cell. Specifically, as the equivalent circuit model of a RH unit cell is a series inductance and a shunt capacitance, the LH unit cell is a series capacitance and a shunt inductance. Thus, the simplest approach to implement a LH TL consists of cascading LH unit cells along the propagation direction. One of the most popular distributed implementations is the one based on the so called ‘‘Sievenpiper’s mushroom structure’’ (for instance, see the structure inside the patch in Fig. 14). This structure is composed of conventional microstrip patches grounded with vias to provide the shunt inductances. The series capacitances are obtained by making separation gaps between the cells. LH TLs have multiple applications in microwave engineering, such as miniaturized and multifrequency circuits [12], [13].

In this Section, metamaterial structures are used to develop simultaneous multifrequency antennas in which size reduction is also achieved. Two different approaches are proposed: the first one is based on filling a conventional microstrip patch with LH structures while the other one consists of coupling metamaterial particles (e. g. SRRs) to the patch.

The first kind patch antennas proposed is based on a novel concept: the simultaneous use of LH and RH modes. On the one hand, conventional patch antennas provide RH modes ( $n > 0$ ). In particular, the  $n = +1$  mode is usually employed [9], [10]. This mode has half-wavelength electrical length and provides a broadside and one beam radiation pattern. On the other hand, some antennas which make use of LH modes ( $n < 0$ ) have been recently proposed to achieve miniaturization [20], [21]. Specifically, the  $n = -1$  mode has an electromagnetic fields distribution similar to the conventional  $n = +1$  mode, but its resonant frequency is below the resonant frequency of a conventional patch. The proposed approach allows obtaining single-port patch antennas in which the  $n = \pm 1$  modes can be used simultaneously and the working frequencies can be chosen within a wide range of values. Moreover, it is also possible to excite simultaneously the  $n = 0$  mode. This mode is achieved in short-circuited patch antennas and it has a uniform electric field distribution (in amplitude and phase) which leads to a monopolar (null at broadside) radiation pattern [22]. Thus, multifunctionality (dual-mode) performance can be also achieved with this first kind of patches.

The second approach (patch antennas with coupled metamaterial particles) is similar to the one proposed for the printed dipoles: additional resonances can be achieved at the self-resonant frequencies of the particles and the conventional resonances are maintained. Thus, multifrequency patch antennas can be obtained by using the conventional and the additional resonances simultaneously.

### 3.1 Patch Antennas Filled with LH Structures

The first kind of multifrequency patch antennas are based on a squared or circular microstrip patch partially filled with LH structures (Fig. 13 (a)). These LH structures can be implemented by using mushroom-type structures. Initially, for simplicity, we can consider propagation along one main direction. In this case, the equivalent antenna TL model is composed of a LH section between two RH sections (Fig. 13 (b)).

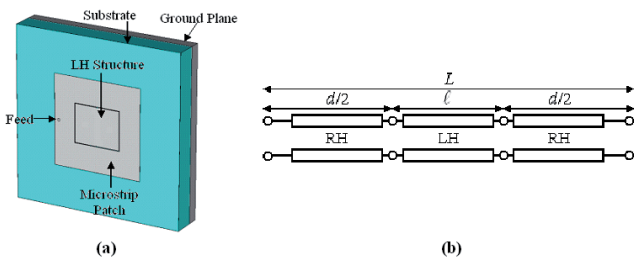


Fig. 13. Microstrip patch filled with LH structures. (a) Sketch of the antenna. (b) Equivalent TL model.

All the EIGs of the antenna satisfy the resonant condition:

$$\beta_n L = n\pi \tag{1}$$

where  $L$  is the equivalent TL length and  $n$  is the resonant index. The propagation constant is positive and linear in

the RH sections and negative and proportional to  $1/\omega$  in the LH sections. Then, the previous condition can be rewritten as:

$$\beta_n L = \beta_n^{RH} d + \beta_n^{LH} \ell = k_1 f_n d - \frac{k_2}{f_n} \ell = n\pi \tag{2}$$

where  $k_1$  and  $k_2$  are constants;  $d$  and  $\ell$  are the equivalent lengths of the RH and LH sections, respectively. In this case, it is possible to obtain modes with negative, zero or positive index, contrary to the conventional patches in which  $n$  is always positive. Specifically, for a LH section composed of  $M$  unit cells,  $n$  takes values:

$$n = -M + 1, -M + 2, \dots, -1, 0, +1, +2, \dots \tag{3}$$

If we take  $M = 2$ , we obtain the  $n = -1$  mode as the fundamental one and avoid undesired lower modes. Moreover, the equivalent mode to the fundamental one of a conventional patch is also present ( $n = +1$ ). For these reasons, a dual-frequency antenna can be developed by using  $n = \pm 1$  modes at the same time. Furthermore, the  $n = 0$  mode is achieved at a frequency between those of the half-wavelength modes. Then, a multifrequency and dual-mode patch antenna can be developed when these three interesting modes ( $n = \pm 1, 0$ ) are excited in a patch antenna filled with LH structures. An example is shown below.

The proposed dual-mode and triple-frequency antenna is shown in Fig. 14 where the patch dimensions ( $L \times W$ ) are 42 mm x 42 mm. The substrate is polypropylene (PP) with  $\epsilon_r = 2.2$  and  $h = 1$  mm. The mushroom structure is based on a  $2 \times 1$  cell array configuration and the dimensions of the mushrooms ( $L_m \times W_m$ ) are 10.6 mm x 17.8 mm. The diameter of the vias ( $d$ ) is 0.7 mm, the gap between the two mushrooms ( $g_1$ ) is 0.40 mm and the separation gap between the microstrip patch and the LH structure ( $g_2$ ) is 0.20 mm. The antenna is fed through a coaxial probe placed 14 mm away from the centre. The dimensions of the ground plane are 80 mm x 80 mm. These dimensions were chosen to obtain the resonant frequencies at 1 GHz (GSM band) for the  $n = -1$  mode, 1.5 GHz (navigation systems) for the  $n = 0$  mode and 2.2 GHz (UMTS band) for the  $n = +1$  mode.

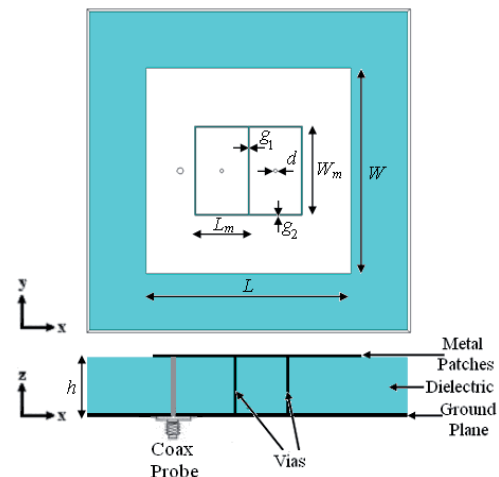
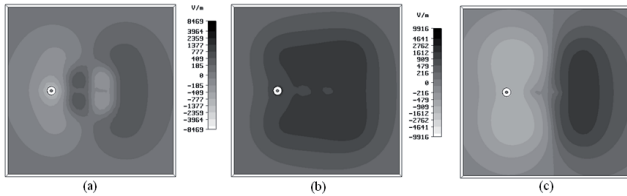


Fig. 14. Sketch of the proposed multifrequency patch antenna filled with LH structures.

The resonance of the  $n = +1$  mode is mainly associated with the patch itself while the lower modes depend on the mushroom structure. Then, the higher frequency ( $n = +1$  mode) will mainly depend on the patch length ( $L$ ), while the resonant frequencies of the other modes can be fixed by choosing the adequate mushroom parameters (basically  $L_m$ ,  $W_m$  and the gaps, because the effect of the vias diameter  $d$  can be neglected). A detailed parametric study has been carried out in [16].

The electric field distributions (CST Microwave Studio) for the modes with  $n = -1$ ,  $n = 0$  and  $n = +1$  indices are shown in Fig. 15. The left handed performance is seen by a local  $180^\circ$  phase shift in the mushroom structure at  $f_{-1}$ , but this singularity does not affect the radiation behavior, as it will be shown in the radiation pattern of the experimental results. On the other hand, the right handed performance can also be seen in the field distribution since it is the same as the fundamental mode of a conventional patch antenna at  $f_{+1}$  and does not present any local phase shift. Lastly, the electric field is constant at  $f_0$ , as was predicted.



**Fig. 15.** Electric field distributions for the proposed antenna: (a)  $n = -1$  mode ( $f_{-1} = 1.06$  GHz), (b)  $n = 0$  mode  $f_0 = 1.45$  GHz), (c)  $n = +1$  mode  $f_{+1} = 2.16$  GHz).

A prototype of this patch antenna has been manufactured (Fig. 16 (a)). Fig. 16 (b) shows the measured reflection coefficient. The return losses are  $-12.62$  dB at  $f_{-1} = 1.06$  GHz,  $-12.01$  dB at  $f_0 = 1.45$  GHz and  $-9.59$  dB at  $f_{+1} = 2.16$  GHz. The ratio between the resonant frequencies of the first and second modes is 1.37 and the ratio between the two dipolar modes is 2.04. The ratio between these modes can be arbitrarily chosen and depends on the patch and mushrooms dimensions, as explained before. The patch length is  $\lambda_0/6.74$  at  $f_{-1}$ ,  $\lambda_0/4.92$  at  $f_0$  and  $\lambda_0/3.31$  at  $f_{+1}$ . It can be seen that a multifrequency antenna with different radiation modes has been obtained. Moreover, the length is strongly reduced with respect to the conventional  $\lambda/2$  patch antennas at the lower frequency.

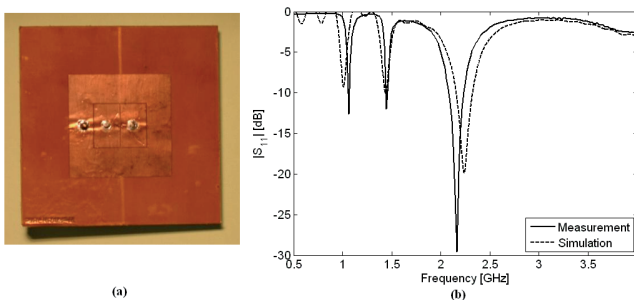


**Fig. 16.** (a) Picture of the triple-frequency and dual-mode patch antenna. (b) Simulated and measured reflection coefficient of the proposed antenna.

Finally, Fig. 17 shows the measured radiation patterns of the E-plane ( $x$ - $z$  plane) and H-plane ( $y$ - $z$  plane) and their corresponding cross polar components. For the  $n = -1$  mode (1.06 GHz) a dipolar pattern can be seen in Fig. 17 (a). The radiation pattern of the  $n = 0$  mode (1.45 GHz) is monopolar as it can be seen in Fig. 17 (b). A null in the broadside direction is appreciated. The depth of this null is 16 dB for the E-plane radiation pattern and 15 dB for the H-plane pattern. Two comments must be made concerning the  $n = 0$  mode. First, the maximum of the radiation pattern that would be in the endfire direction is somewhat reduced due to the effect of the finite ground plane. Secondly, the  $n = 0$  mode is excited in a weaker way than the  $n = 0$  mode in a short circuited patch antenna [22]. This can be seen because of the higher level of the cross polar component. The broadside radiation pattern is also achieved for the  $n = +1$  mode (2.16 GHz, Fig. 17 (c)). The measured gain of the antenna is  $-3$  dB at  $f_{-1}$ , 1 dB at  $f_0$  and 6.5 dB at  $f_{+1}$ . The gain of the additional modes ( $n = -1, 0$ ) is reduced with respect to conventional patches because the electrical length of the patch antenna is also smaller due to the miniaturization achieved.

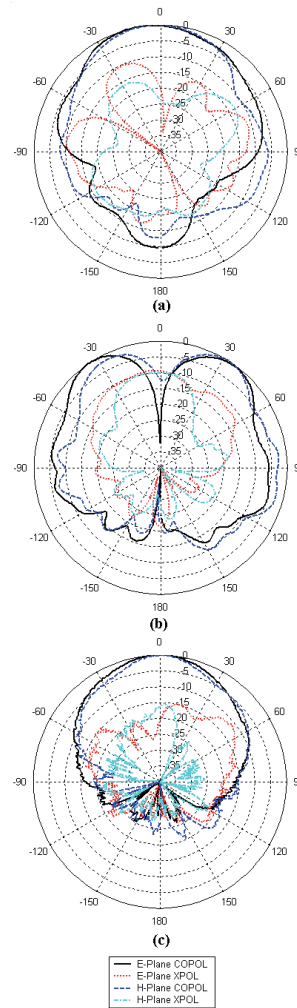


**Fig. 17.** Measured radiation patterns of the triple-frequency and dual-mode patch antenna. (a)  $n = -1$  mode ( $f_{-1} = 1.06$  GHz), (b)  $n = 0$  mode  $f_0 = 1.45$  GHz), (c)  $n = +1$  mode  $f_{+1} = 2.16$  GHz).

### 3.2 Multifrequency Patch Antennas Loaded with Metamaterial Particles

As it has been demonstrated in the previous Subsection, the use of mushroom-type LH structures allows multifrequency performance in patch antennas working in the low-GHz band (below 3 GHz), even when the ratio between the working frequencies is very small. The same approach has been applied to multifrequency patch antennas working at higher frequencies (e. g. X-band). However, some difficulties have been found for some applications in which the ratios between the working frequencies are extremely small ( $< 1.4$ ): the mushrooms are very large to fit them inside the patches. Moreover, very high resolution is needed to implement the gaps and vias of the mushroom structures. The second kind of patch antennas can be used to overcome these difficulties. Several examples of patch antennas loaded with metamaterial particles (in particular SRRs) are shown below. This second proposal has another interesting feature: the possibility of achieving multifrequency (more than two working frequencies) with patch-like radiation patterns. This new kind of antennas avoids using non-planar elements such as vias.

The proposed dual-frequency antenna loaded with SRRs is shown in Fig. 18 (a). It consists of a conventional square patch antenna with two SRRs placed close to and coplanar to the patch. Both the patch and the SRRs can be simultaneously excited by feeding the patch correctly, exhibiting each element a different resonant frequency. The geometry of the SRRs is square in order to increase the coupling between the patch and the particles. A planar dual-frequency antenna can be achieved, in which the working frequencies can be arbitrarily chosen by changing the dimensions of the patch or the SRRs. One of the working frequencies is due to the patch itself and the other is due to the self-resonance of the SRRs. At both working frequencies the radiating element is the patch, so the antenna presents a broadside radiation pattern. It is important to note that the additional resonances can be placed above or below the resonant frequency of the patch.

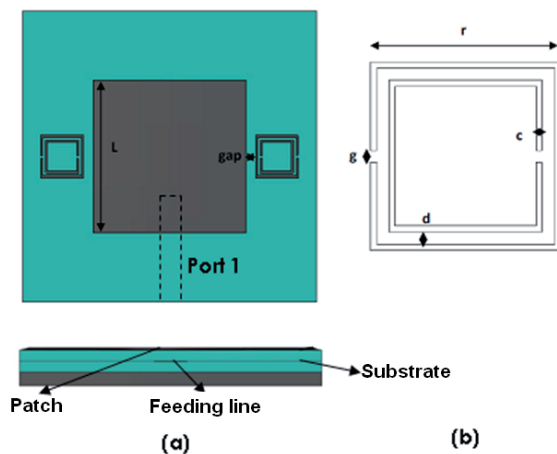


Fig. 18. (a) Sketch of the patch antenna loaded with SRRs. (b) Design parameters of a square SRR.

The first designed, simulated and manufactured prototype is a dual-frequency antenna with linear polarization working in the X-Band at 7.71 GHz and 8.33 GHz. The dimensions of the antenna, following the labels in Fig. 18, are:  $L = 10.9$  mm,  $gap = 0.7$  mm,  $r = 3.2$  mm,  $c = 0.15$  mm,  $d = 0.2$  mm and  $g = 0.2$  mm. The feeding technique is a proximity coupled microstrip line [9], so two substrates are used. Both substrates are Rogers RT Duroid 5880 with a thickness of 0.787 mm and  $\epsilon_r = 2.2$ . Simulations have been undertaken with CST Microwave Studio and the prototype is shown in Fig. 19. The reflection coefficient parameter ( $|S_{11}|$ ) has been measured and the results are very similar to those obtained in the simulation (Fig. 20). The measured resonant frequencies are 7.71 GHz and 8.33 GHz.

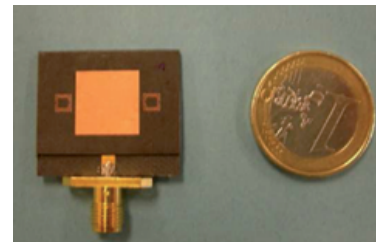


Fig. 19. Manufactured dual-frequency patch antenna loaded with SRRs.

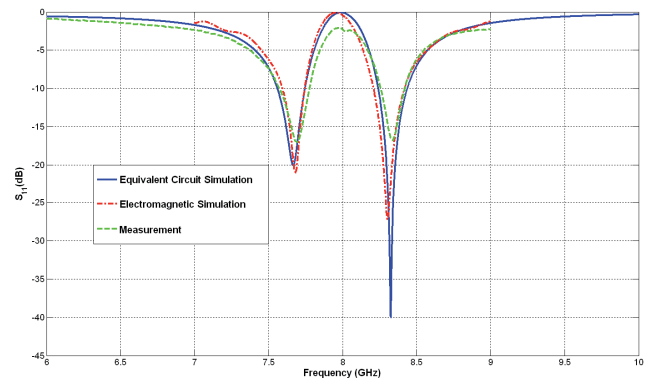


Fig. 20. Measured and simulated reflection coefficients of the dual-frequency patch antenna loaded with SRRs. The simulations have been carried out with an electromagnetic simulator (CST Microwave Studio) and the proposed equivalent circuit model.

The simulated radiation patterns obtained are shown in Fig. 21. The radiation patterns are broadside and very similar to the conventional patch radiation pattern. The directivity is 6.1 dB at 7.71 GHz and 6.6 dB at 8.33 GHz. Radiation efficiency is closed to 95% at both frequencies.

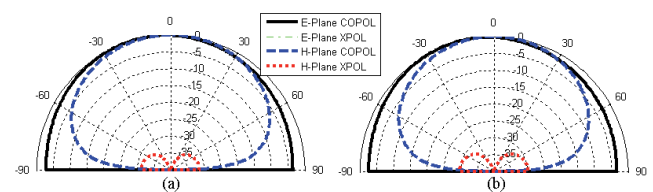


Fig. 21. Simulated radiation pattern of the proposed dual-frequency patch antenna loaded with SRRs. (a) 7.71 GHz. (b) 8.33 GHz.

The proposed approach can be easily extended to the design of multifrequency patch antennas with more than two working frequencies. Additional SRRs with different resonant frequencies can be placed at both sides of the patch. As an example, a triple-frequency patch antenna is proposed below.

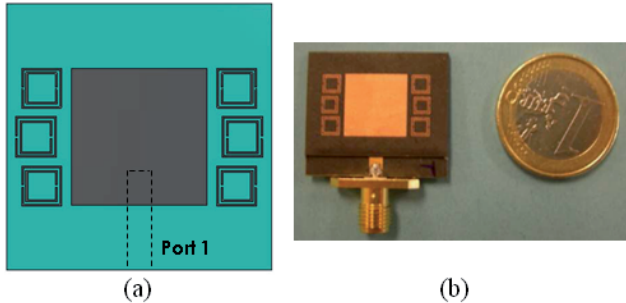


Fig. 22. (a) Sketch of the multifrequency patch antenna loaded with SRRs. (b) Picture of the manufactured prototype.

The main idea to achieve the multifrequency performance consists on coupling particles with different resonant frequencies to the patch antenna. Fig. 22 shows three pairs of SRRs coupled to a square patch antenna. The top and bottom pairs are similar, but the SRRs of the central pair have different dimensions in comparison with the other SRRs. Thus, three different resonant frequencies are achieved: the first one is devoted to the central pair of SRRs, the second one is due to the remaining SRRs while the other one is the  $n = +1$  mode resonant frequency of the patch itself.

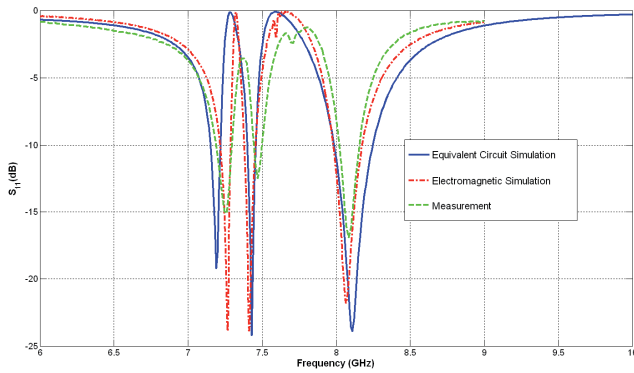


Fig. 23. Measured and simulated reflection coefficients of the triple-frequency patch antenna loaded with SRRs. The simulations have been carried out with an electromagnetic simulator (CST Microwave Studio) and the proposed equivalent circuit model.

The dimensions of the proposed prototype are  $L = 11.3$  mm, central SRRs:  $gap = 1.2$  mm,  $r = 3.4$  mm,  $c = 0.15$  mm,  $d = 0.2$  mm,  $g = 0.2$  mm; top and bottom SRRs:  $gap = 0.8$  mm,  $r = 3.3$  mm,  $c = 0.15$  mm,  $d = 0.2$  mm,  $g = 0.2$  mm. The separation between SRRs is 0.7 mm. The manufactured prototype is shown in Fig. 22 (b) and the simulated and measured results are shown in Fig. 23. The measured working frequencies are 7.26 GHz, 7.48 GHz and 8.09 GHz. It is important to note that the resonant

frequencies can be chosen arbitrarily and the ratio between any pair of them is different.

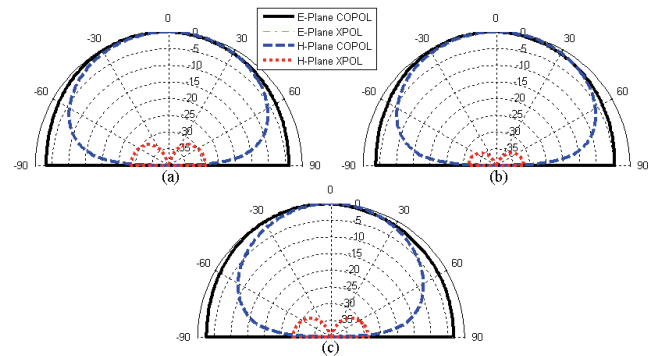


Fig. 24. Simulated radiation pattern of the proposed triple-frequency patch antenna loaded with SRRs. (a) 7.26 GHz. (b) 7.48 GHz. (c) 8.09 GHz.

The simulated radiation patterns at the three working frequencies are shown in Fig. 24. The computed directivities and radiation efficiencies are 6.06 dB and 89%, 6.2 dB and 89.6%, 6.75 dB and 91.73% at 7.26 GHz, 7.48 GHz and 8.09 GHz, respectively.

An equivalent circuit model of patch antennas with coupled SRRs is proposed in Fig. 25. The patch antenna with resonant frequency  $f_0$  ( $n = +1$  mode) is modeled as a transmission line with length  $L \approx \lambda_0/2$  and width  $W$ . Resistances and capacitors at the ends of the patch are used to model the radiated and the stored fields in the proximity of the patch, respectively. As in Section 2.2, SRRs are modeled as a LC parallel tank circuit whose resonant frequency is given by  $\omega_0 = (L_{SRR}C_{SRR})^{-1/2}$ . The LC parallel tank corresponding to the SRRs is coupled to the patch through a mutual inductance, which models the magnetic coupling between the elements. Additional coupled LC parallel tanks must be added to the model when SRRs with different self-resonant frequencies are used, as in the triple-frequency presented before.

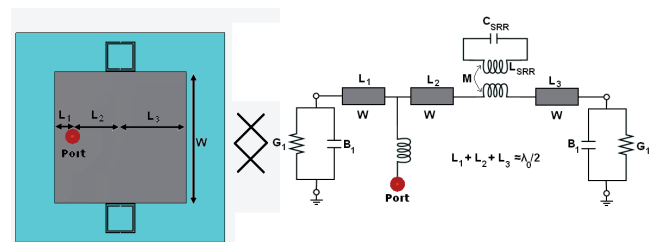


Fig. 25. Equivalent circuit model of the metamaterial-loaded patch antennas.

The two prototypes presented previously (dual-frequency and triple-frequency patch antennas loaded with SRRs) have been simulated with the proposed model and a full-wave electromagnetic simulator (CST Microwave Studio) to validate the proposed model. There is an excellent agreement between the different results (Fig. 20 and Fig. 23).

## 4. Applications

In the previous chapters, several multifrequency metamaterial based antennas have been proposed. For most of the cases different prototypes working at the frequencies of different communications systems have been designed. For example, the multifrequency patch antennas were designed for the frequencies of mobile communications systems (GSM, DCS and UMTS) and radio navigation systems (GPS). Thus, these antennas can be used as radiating elements of portable devices for the proposed services. Moreover, they have been also proposed for satellite applications (X-Band).

The aim of this Section is to study the application of the metamaterial based antennas not as isolated radiating elements, but integrated into systems or antenna arrays. Moreover, novel antennas are proposed to fulfill the requirements of emerging applications such as RFID. A novel scheme for active RFID systems based on self-diplexed multifrequency patch antennas (multi-port patch antennas with high isolation between the ports working at two frequencies) is proposed (Section 4.1).

The proposed antennas can be used to enhance the performance of antenna arrays. In Section 4.2 the dual-band dipoles are used to design log-periodic arrays of printed dipoles with interesting features such as miniaturization or bandwidth broadening with respect to conventional log-periodic arrays.

### 4.1 Self-Diplexed Patch Antennas for Active RFID Systems

RFID systems have grown very fast in the last years for automatic identification of objects by RF signals means [11]. RFID systems can be classified according to their fundamental parameters such as working frequency, range, electromagnetic coupling, and type of communication between reader and transponder, type of access and active or passive systems. Basically it can be said that an RFID system is composed of two devices: the transponder and the reader. The reader transmits a modulated signal with periods of unmodulated carrier.

This is received by the transponder (or tag) that consists of an antenna and an application specific integrated circuit (ASIC) chip. The transponder modulates the received signal with its identification code and sends back the information.

Microwave bands (i.e. 2.45 GHz) are being used more and more for RFID systems [11]. Passive RFID systems use the same frequency for both radio-links: the reader-transponder link and the transponder-reader link. This approach hinders the design of the reader and it requires higher transmission power from the transponder to allow a proper information reception at the reader side. This implies that the system must be half-duplex and that the transponder-reader link is power limited due to the very

small power that can be generated by the tag itself. As the power generated by the tag is limited, great efforts have been undertaken in the antenna design in order to look for a proper conjugate impedance match between the antenna and the chip. In this way the energy transfer between the antenna and the transponder would be optimal. Resonant antennas present a large impedance variation around the resonant condition. This fact makes resonant antennas (e. g. patch antennas) suitable to achieve conjugate impedance matching without any matching network.

The use of self-diplexed multifrequency resonant antennas [23], [24] would make more suitable the design of readers and transponders compatible with both half and full-duplex communications. In addition, it also allows working with active RFID systems what increases the capabilities of the system (e. g. larger detection ranges). An optimal solution could be that reader-transponder link would work at a frequency  $f_0$  while the transponder-reader link would work at an anharmonic lower frequency ( $f_0 / n$ , where  $n$  is an arbitrary number not forced to be an integer number). This fact would reduce the losses in the power restricted link while diminishing the power requirements in the transponder and optimizing the range performance. The proposed active RFID system implements this solution [24] and is summarized below.

The proposed active RFID system is shown in Fig. 26. The antennas are patches partially filled with LH cells. This allows having a dual-frequency antenna. Moreover, the antennas must be self-diplexed (multi-port antennas with high isolation between the ports) to be connected directly to the transmitters and receivers without any interference. The transponder antenna is a linearly polarized one that receives at  $f_2$  (the higher frequency) while transmits at  $f_1$  (the lower frequency) in order to reduce the propagation losses in the most critical link (transponder-reader). In addition, the transponder antenna must provide a conjugate complex impedance to have the lowest mismatching factor and achieve the maximum power transfer.

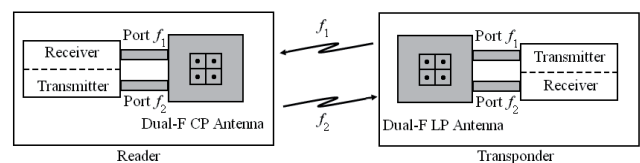


Fig. 26. Proposed architecture for the RFID active system based on self-diplexed antennas filled with metamaterials.

The reader antenna is a circularly polarized one that transmits at  $f_2$  (the higher frequency) while receives at  $f_1$  (the lower frequency) in order to overcome the multipath problems and reduce the polarization losses and the link fading. In this case the antenna impedance is matched to the front-end impedance ( $Z_0$ ). Thus, in this case the design is somewhat different as in the transponder case.

The proposed antennas are based on the multifrequency patch antennas filled with LH structures presented

in Section 3.1, but some considerations must be taken into account in order to use them for the proposed RFID system. First of all, the most adequate feeding technique must be chosen by taking into account the different requirements of the two elements which compose the RFID system (reader and transponder). Moreover, an approach to obtain the self-diplexing capability must be developed.

Regarding to the feeding consideration, two types of feeding approaches are proposed. The first one is the use of a proximity coupled line and the second one is the use of a line coupled to the patch through a slot in the ground plane. The first approach is easier to implement, but it only provides one parameter to match the antenna. This parameter is the depth of the feeding line under the patch. On the other hand, the coupled line through a slot approach has more degrees of freedom (the dimensions of the slot, the position of the slot and the depth of the line) but this approach is more difficult to implement and more expensive, because another substrate is needed to print the coupled line under the ground plane. For this reason, the first approach has been proposed to match the reader antenna to the front-end. The second approach has been proposed for the transponder antennas because it provides more degrees of freedom to match the antenna and reduce the mismatch between the antenna and the ASIC.

The proposed approach to achieve the desired self-diplexing performance is the use of filtering feeding lines. This technique consists of coupling metamaterial filtering particles to the feeding lines. These particles have a pass-band characteristic at the working frequency of the port, enhancing the isolation between the different ports. Moreover, the use of these filtering lines does not increase the total dimensions of the antenna. A sketch of a self-diplexed antenna with orthogonal polarizations is shown in Fig. 27.

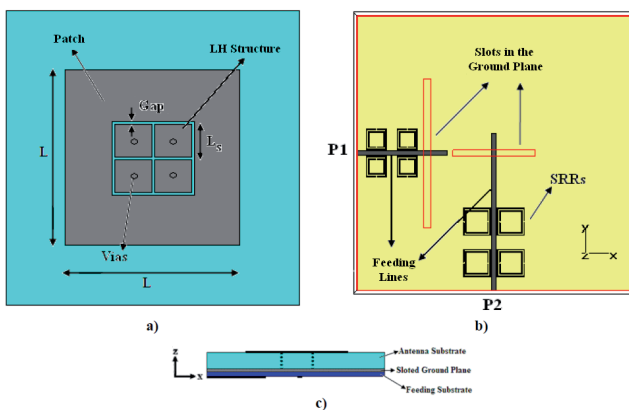


**Fig. 27.** Sketch of a self-diplexed antenna for a RFID transponder. (a) Top view. (b) Feeding approach. (c) Side view.

Two self-diplexed, dual-frequency, linearly polarized antennas for the transponder have been designed, manufactured and measured: one with equal polarized output ports and other with orthogonal polarized ports (Fig. 28 (a)-(b)). Isolation levels larger than 31 dB for the equally polarized antenna and larger than 40 dB for the orthogonal

one has been achieved. Another dual-frequency, circularly polarized, self-diplexed antenna has been manufactured for the reader antenna (Fig. 28 (c)). Isolation levels larger than 35 dB have been achieved [24].

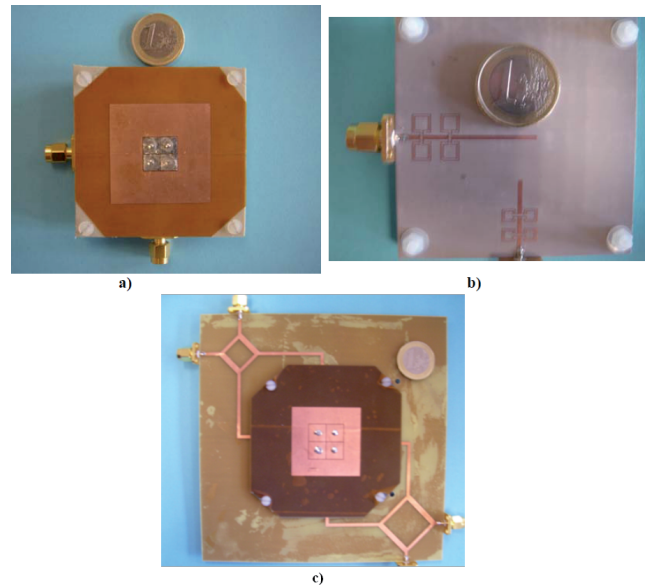


**Fig. 28.** Pictures of the self-diplexed prototypes for RFID application. (a) Top view of a linearly polarized self-diplexed antenna for a RFID transponder. (b) Bottom view of a linearly polarized self-diplexed antenna for a RFID transponder. (c) Top view of the circularly polarized self-diplexed antenna for a RFID reader.

## 4.2 Arrays of Dual-Band Printed Dipoles Loaded with Metamaterial Particles

The aim of this Subsection is the study of arrays of dual-band printed dipoles loaded with metamaterial particles. In particular, the log-periodic configuration is proposed. A log-periodic array composed of these dipoles can provide interesting features:

- Array miniaturizing: this is possible by substituting some dipoles of the array by the additional resonances of dual-band dipoles. Thus, the number of physical dipoles forming the array is reduced.
- Array bandwidth broadening: this approach consists of including additional resonances below or/and above the bandwidth of the overall antenna in order to broaden it.

An example of the later is proposed in this Section. The dual-band dipole implementation is based on the printed dipoles loaded with Omega particles presented in Section 2.1. The reference antenna is the simplest log-periodic array: the one composed of two dipoles (Fig. 29 (a)). These dipoles are implemented by using an antipodal configuration (each branch of the dipole is printed on one side of a dielectric substrate; the dipole is fed through a parallel plate line). The substrate is FR-4 ( $\epsilon_r=4.50$  and  $\tan\delta=0.015$ ) with 0.50 mm thickness. The dimensions of the dipoles are

$L_1= 28.50$  mm,  $L_2= 32.00$  mm,  $W_1=3.00$  mm,  $W_2=4.00$  mm,  $D_1= 19.75$  mm,  $D_2= 25.00$  mm,  $W_f= 1.00$  mm. Fig. 29 (b) shows the reflection coefficient of the dipoles and the log-periodic array. The resonant frequencies of the isolated dipoles are:  $f_1 = 2.12$  GHz and  $f_2 = 1.93$  GHz. The bandwidth of the dipoles is 12% approximately. The log-periodic array has a reflection coefficient smaller than  $-10$  dB from 1.70 GHz to 2.57 GHz (40% bandwidth).

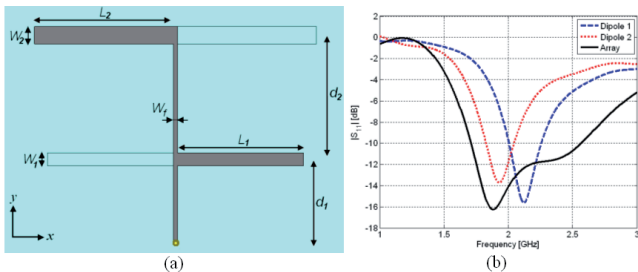


**Fig. 29.** Log-periodic array of two antipodal printed dipoles. (a) Top view. (b) Simulated reflection coefficient of the array and the isolated dipoles.

The strategy to broaden the bandwidth of the reference dipole array is to obtain two additional resonances. One of the additional resonances is placed below the resonances of the original array and the other one above its frequency bandwidth. Moreover, the number of the dipoles is maintained; thus, the dimensions of the array are not increased. In order to achieve these goals, dual-frequency dipoles loaded with metamaterial particles are used. The dipoles of the reference log-periodic array are loaded with the Omega particles (Fig. 5), as shown previously. The first dipole is the one presented in Section 2.1. The dimensions of the Omega particles coupled to the second dipole are:  $L_p = 3.80$  mm,  $W_p = 3 \cdot L_p$ ,  $W_s = 0.40$  mm. The separation gap between the dipoles and the particles is 0.20 mm. The particles are placed at the centre of each branch of the dipoles.

The reflection coefficients (computed with CST Microwave Studio) of the dual-band dipoles and the proposed log-periodic array are shown in Fig. 30. The dipoles have the desired dual-band operation. The first dipole has the additional resonance at 1.70 GHz, as it was demonstrated previously. The resonant frequencies of the second loaded dipole are 1.83 GHz and 2.35 GHz. Thus, the bandwidth of the array (reflection coefficient smaller than  $-10$  dB) goes from 1.58 GHz to 2.69 GHz (52% bandwidth). The bandwidth of the proposed array is broader than the conventional one. Moreover, the lower-limit frequency has been shifted down and the upper-limit frequency has been shifted up without increasing the number of dipoles.

Prototypes of the reference and the proposed antennas have been manufactured (Fig. 31 (a)-(b)). Fig. 31 (c) shows the measured reflection coefficient of both antennas. The bandwidth of the reference array goes from 1.62 GHz to 2.77 GHz. In the case of the proposed antenna, it goes from 1.55 GHz to 2.97 GHz. Thus, the bandwidth of the proposed antenna (62.8% BW) has been increased with respect to the reference one (52.4% BW).

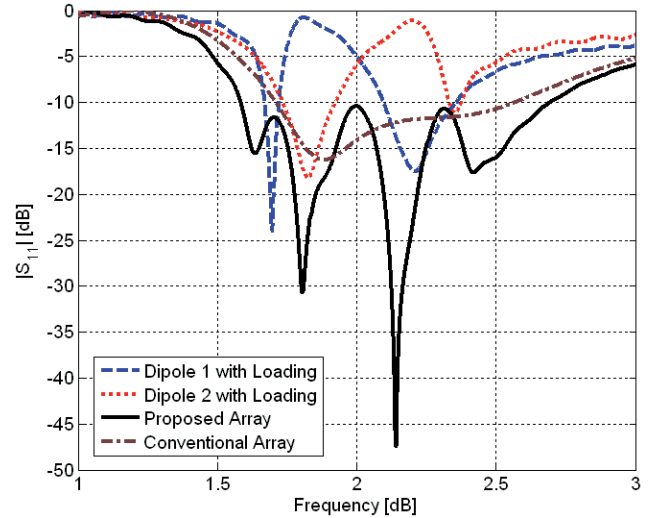


**Fig. 30.** Simulated reflection coefficients of the loaded dipoles and array. The reflection coefficient of the conventional array is also plotted.

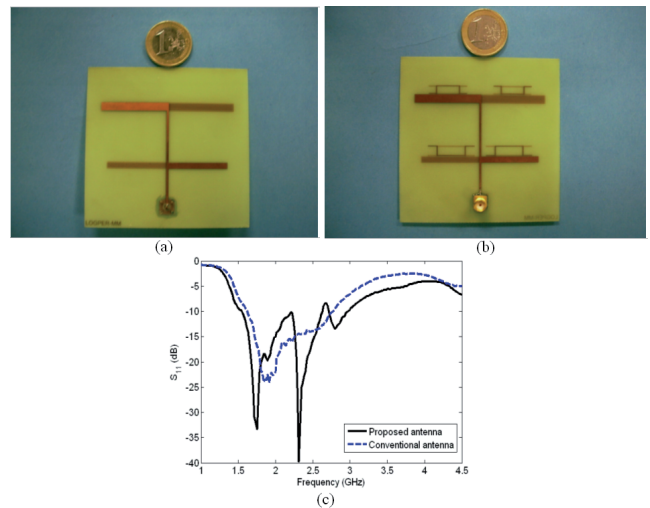


**Fig. 31.** Manufactured prototypes of the log-periodic arrays. (a) Picture of the conventional array. (b) Picture of the proposed array. (c) Measured reflection coefficient of both antennas.

## 5. Conclusions

Metamaterial-loaded printed antennas have been reviewed. As it has been shown, this kind of antennas provides interesting features such as multifrequency, multifunctionality and compactness which are fundamental for modern communication systems. Moreover, the advantages of printed antennas (light weight, low profile, low cost, easiness of manufacturing, etc.) are maintained. Several models based on TL theory and equivalent circuits have been reviewed. These models provide accurate results and a small computation time. Finally, it has been shown that the proposed antennas are a good candidate as the radiating elements of emerging applications such as active RFID systems.

## Acknowledgements

This work was partially granted by the Spanish MEC under Projects TEC2006-13248-C04-04/TCM and TEC2007-65214/TCM. F. J. Herraiz-Martínez is recipient of an official grant (FPU Program) from the Spanish Science and Innovation Ministry (MICINN) to fund his research activity.

## References

- [1] DOWLA, F. *Handbook of RF and Wireless Technologies*. Newnes, 2004.
- [2] LIU, Z. D., HALL, P. S., WAKE, D. Dual-frequency planar inverted-F antenna. *IEEE Transactions on Antennas and Propagation*, 1997, vol. 54, no. 10, pp. 1451-1458.
- [3] MARTÍNEZ-VÁZQUEZ, M., LITSCHKE, O., GEISLER, M., HEBERLING, D., MARTÍNEZ-GONZÁLEZ, A. M., SÁNCHEZ-HERNÁNDEZ, D. Integrated planar multiband antennas for personal communication handsets. *IEEE Transactions on Antennas and Propagation*, 2006, vol. 54, no. 2, part 1, pp. 384-391.
- [4] Special Issue on Multifunction Antennas and Antenna Systems. *IEEE Transactions on Antennas and Propagation*, 2006, vol. 54, no. 2.
- [5] EKSTROM, H., FURUSKAR, A., KARLSSON, J., MEYER, M., PARKVALL, S., TORSNER, J., WAHLQVIST, M. Technical solutions for the 3G long-term evolution. *IEEE Communications Magazine*, 2006, vol. 44, no.3, pp- 38-45.
- [6] IEEE 802.11 n/D9, March 2009.
- [7] KUMAR, G, RAY, K. P. *Broadband Microstrip Antennas*. Artech House, 2003.
- [8] WONG, K.-L. *Compact and Broadband Microstrip Antennas*. John Wiley & Sons, 2002.
- [9] GARG, R., BHARTIA, P., BAHL, I., ITTIPIBOON, A. *Microstrip Antenna Design Handbook*. Norwood: Artech House, 2001.
- [10] JAMES, J. R., HALL, P. S. *Handbook of Microstrip Antennas*. London: Peter Peregrinus, 1989.
- [11] FINKENZELLER, K. *RFID Handbook: Fundamentals and Application in Contactless Smart Cards and Identification*. New York: John Wiley & Sons, 2003.
- [12] MARQUÉS, R., MARTÍN, F., SOROLLA, M. *Metamaterials with Negative Parameters*. Hoboken, NJ: John Wiley & Sons, 2007.
- [13] CALOZ, C., ITOH, T. *Electromagnetic Metamaterials: Transmission Line Theory and Microwave Applications*. New York: Wiley, 2004.
- [14] ELEFThERIADES, G. V., BALMAIN, K. G. *Negative-Refractive Metamaterials: Fundamental Principles and Applications*. Wiley-IEEE Press, July 2005.
- [15] ENGHETA, N., ZIOLKOWSKI, R. W. *Metamaterials: Physics and Engineering Explorations*. Wiley-IEEE Press, August 2006.
- [16] HERRAIZ-MARTÍNEZ, F. J., GARCÍA-MUÑOZ, L. E., GONZÁLEZ-POSADAS, V., SEGOVIA-VARGAS, D. Multi-frequency and dual mode patch antennas partially filled with Left-Handed structures. *IEEE Transactions on Antennas and Propagation*, 2008, vol. 58, no. 8, part 2, pp. 2527-2539.
- [17] HERRAIZ-MARTÍNEZ, F. J., GARCÍA-MUÑOZ, L. E., GONZÁLEZ-OVEJERO, D., GONZÁLEZ-POSADAS V., SEGOVIA-VARGAS D. Dual-frequency printed dipole loaded with Split Ring Resonators. *IEEE Antennas and Wireless Propagation Letters*, 2009, vol. 8, pp. 137-140.
- [18] WADELL, B.C. *Transmission Line Design Handbook*. Norwood, MA: Artech House, 1991.
- [19] BAENA, J. D., BONACHE, J., MARTÍN, F., MARQUÉS, R., FALCONE, F., LOPETEGUI, T., G. LASO, M. A., GARCÍA, J., GIL, I., SOROLLA, M. Equivalent circuit models for split ring resonators and complementary split ring resonators coupled to planar transmission lines. *IEEE Transactions on Microwave Theory and Techniques*, 2005, vol. 53, pp. 1451-1461.
- [20] SCHÜBLER, M., FREESE J., JAKOBY, R. Design of compact planar antennas using LH Transmission Lines. *Proc. IEEE MTT-S Int. Microwave Symp.*, vol. 1, pp. 209-212, June 2004.
- [21] LEE, C. J., LEONG, K. M. K. H., ITOH, T. Composite Right/Left-Handed Transmission Line based compact resonant antennas for RF module integration. *IEEE Transactions on Antennas and Propagation*, 2006, vol. 54, no. 8, pp. 2283-2291.
- [22] GONZÁLEZ-POSADAS, V., SEGOVIA-VARGAS, D., RAJO-IGLESIAS, E., VÁZQUEZ-ROY, J. L., MARTÍN-PASCUAL, C. Approximate analysis of short circuited ring patch antenna working at TM<sub>01</sub> mode. *IEEE Transactions on Antennas and Propagation*, 2006, vol. 54, no. 6, pp. 1875-1879.
- [23] UGARTE-MUÑOZ, E., HERRAIZ-MARTÍNEZ, F. J., GONZÁLEZ-POSADAS, V., SEGOVIA-VARGAS, D. Patch antenna based on metamaterials for a RFID transponder. *Radioengineering*, June 2008, vol. 17, no. 2, pp. 66 – 71.
- [24] HERRAIZ-MARTÍNEZ, F. J., UGARTE-MUÑOZ, E., GONZÁLEZ-POSADAS, V., GARCÍA-MUÑOZ, L. E., SEGOVIA-VARGAS, D. Self-diplexed patch antennas based on metamaterials for active RFID systems. *IEEE Transactions on Microwave Theory and Techniques, Special Issue on RFID*, May 2009, vol. 57, no. 5, part 2, pp. 1330 – 1340.

## About Authors ...

**Daniel SEGOVIA-VARGAS** was born in Madrid in 1968. He received the Telecommunication Engineering Degree and the Ph.D. from the Polytechnic University of Madrid in 1993 and in 1998. From 1993 to 1998 he was an Assistant Professor at Valladolid University. From 1998 he is an Associate Professor at Carlos III University in Madrid where he is in charge of the Microwaves and Antenna courses. He has authored and co-authored over 90 technical conference, letters and journal papers. His research areas are printed antennas and active radiators and arrays and smart antennas, LH metamaterials, passive circuits and RFID systems. He has also been member of the European Projects Cost260, Cost284 and COST IC0603.

**Francisco Javier HERRAIZ-MARTÍNEZ** was born in Cuenca, Spain, on May 3, 1983. He received the Engineer degree in telecommunications from Carlos III University in Madrid, Spain, in 2006 (awarded with the first prize). He is currently working towards the Ph.D. in communications at Carlos III University in Madrid. His research interests include active antennas, metamaterial applications for antenna and microwave circuits and RFID systems. Mr. Herraiz-Martínez received the Best Master Thesis Dissertation Award from the COIT/AEIT in 2006. He was finalist of the IEEE AP-S Student Paper contest in 2007. He is

recipient of a Spanish Education and Science Ministry (MEC) official grant for funding his research activity.

**Eduardo UGARTE-MUÑOZ** was born in Caracas, Venezuela on April 23, 1983. He received the Engineer degree in telecommunications from the Carlos III University in Madrid, Spain, in 2008. He is currently working towards the Ph.D. in communications at Carlos III University in Madrid. His research lines are metamaterials, RFID systems and active antennas.

**Javier MONTERO-DE-PAZ** was born in Madrid, Spain, on May 29, 1984. He received the Engineer degree in telecommunications from Carlos III University, Madrid, Spain, in 2009, and is currently working toward the Ph.D. degree in communications at Carlos III University. His research lines are metamaterials, active antennas, and terahertz antennas.

**Vicente GONZÁLEZ-POSADAS** was born in Madrid (Spain) in 1968. He received the Ing. Técnico in radio-communication engineering degree from the Polytechnic

University of Madrid (UPM) in 1992, M.S. degree in physics in 1995, from the UNED and Ph.D degree in telecommunication engineering in 2001 from the Carlos III University of Madrid. He is working now as an Assistant Professor at the Technical Telecommunication School in the Polytechnic University of Madrid. His interests are related to active antennas, microstrip antennas, CRLH lines and metamaterials, microwave technology and RFID. He has authored or coauthored over 60 technical conference, letter and journal papers.

**Luis Enrique GARCÍA-MUÑOZ** received the telecom engineer degree from Universidad Politécnica de Madrid, Spain, in 1999 and the Ph.D. degree in telecommunication from the Universidad Politécnica de Madrid, Madrid, Spain, in 2003. He is an Associate Professor with the Department of Signal Theory and Communications, University Carlos III, Madrid. His main research interests include radioastronomy receivers, radiotelescopes, microstrip patch antennas and arrays as well as periodic structures applied to electromagnetics.